OPEN ACCESS

Complex magnetism of the Fe monolayer on Ir(111)

New Journal of Physics
The open-access journal for physics

Complex magnetism of the Fe monolayer on Ir(111)

Kirsten von Bergmann[1,3], Stefan Heinze[1], Matthias Bode[1], Gustav Bihlmayer[2], Stefan Blügel[2] and Roland Wiesendanger[1]

[1] Institute of Applied Physics, University of Hamburg, Jungiusstraße 11, 20355 Hamburg, Germany
[2] Institut für Festkörperforschung, Forschungszentrum Jülich, 52425 Jülich, Germany
E-mail: kbergman@physnet.uni-hamburg.de

New Journal of Physics **9** (2007) 396
Received 31 May 2007
Published 31 October 2007
Online at http://www.njp.org/
doi:10.1088/1367-2630/9/10/396

Abstract. The electronic and magnetic properties of Fe on Ir(111) have been investigated experimentally by spin-polarized scanning tunneling microscopy (SP-STM) and theoretically by first-principles calculations based on density functional theory. While the growth of an Fe monolayer is in-plane commensurate, deposition of a double-layer shows a rearrangement of atoms due to strain relief accompanied by local variations of the electronic structure. Both stackings of the monolayer, i.e. face centered cubic (fcc) and hexagonal closed packed (hcp), are observed experimentally. The magnetic structure of both types is imaged with SP-STM. From these experiments, we propose a nanoscale magnetic mosaic structure for the fcc-stacking with 15 atoms in the unit cell. For hcp-stacking, the tunneling spectra are similar to the fcc case, however, the magnetic contrast in the SP-STM images is not as obvious. In our first-principles calculations, a collinear antiferromagnetic (AFM) state with a 15 atom in-plane unit cell (AFM 7 : 8 state) is found to be more favorable than the ferromagnetic state for both fcc- and hcp-stacking. Calculated SP-STM images and spectra are also in good agreement with the experimental data for the fcc case. We performed spin spiral calculations which are mapped to a classical Heisenberg model to obtain the exchange-interaction constants. From these calculations, it is found that the AFM 7 : 8 state is energetically more favorable than all solutions of the

[3] Author to whom any correspondence should be addressed.

PII: S1367-2630(07)51847-1

classical Heisenberg model. While the obtained magnetic exchange constants are rather similar for the fcc and hcp stacking, a comparison with the experiments indicates that competing interactions could be responsible for the differences observed in the magnetically sensitive measurements.

Contents

1. Introduction

Driven by the demand to fabricate magnetic structures on increasingly smaller length scales, magnetism in reduced dimensions is a topic of fundamental and practical relevance. While spatially averaging techniques have a long tradition in the investigation of magnetism [1]–[5], the major drawback of limited spatial resolution is obvious: especially when antiferromagnetic (AFM) or complex magnetic structures occur, these methods may not be sufficient, since the probed sample volume is in these cases usually larger than one magnetic unit cell. In addition, a system with largely compensated magnetic moments might not respond to magnetic fields readily available in standard laboratory equipment, thus one parameter to comfortably induce changes in the sample cannot be exploited. Furthermore, these conventional methods do not only lack spatial resolution, but they usually also have sensitivity problems when the amount of magnetic material is reduced.

However, the investigation of small magnetic structures—by experiment as well as by theory—is essential for the understanding of fundamental aspects of magnetic interactions as well as for the design of functional materials and tuning of their magnetic properties. It is well known that the local surrounding of the magnetic atoms in a sample has a large influence on the magnetic properties: for instance Fe—which is ferromagnetic (FM) in the bulk with body-centered cubic (bcc) structure—was found to have a spin spiral (SS) ground state when it is in a face-centered cubic (fcc) environment [6, 7], or can even show a checkerboard AFM structure when deposited as a single atomic layer on W(001) [8, 9]. In addition to the symmetry, number and distance of nearest neighbors also the hybridization can play a crucial role for the magnetic properties. Recent theoretical studies have demonstrated that the magnetic state in a monolayer

of Fe can be tuned by changing only the band filling of a 5d transition-metal substrate from FM to AFM, with complex non-collinear phases at the intermediate regime [10].

The investigation of magnetism in thin films and nanostructures on surfaces by spin-polarized scanning tunneling microscopy (SP-STM) has demonstrated the capability of this method to study AFM or even more complex magnetic structures down to the atomic scale [8], [11]–[16]. Even though multi-component [12] or reconstructed [15] samples can be studied with this method, already the investigation of homoatomic monolayers of 3d transition metals on 5d substrates has recently revealed fascinating physics [14, 16] and allows an interpretation of the experimental results based on the atomic scale magnetic structure [17]. While the formation of a FM or AFM state can be the result of a dominating nearest neighbor exchange interaction, complex magnetic structures often reflect a situation of competing magnetic interactions. Exchange interactions in a homoatomic monolayer on a substrate can be described by mapping the results of *ab initio* electronic structure calculations on a two-dimensional (2D) classical Heisenberg model. This makes it possible to search for the origin of a specific magnetic ground state, i.e. to find out which interactions compete or dominate. This, of course, facilitates a general understanding of magnetism and might allow the tailoring of magnetic properties in the future.

Here, we study the system of Fe on the Ir(111) surface using SP-STM and density functional theory. This system can be expected to show interesting magnetic structures due to the modified symmetry of the grown Fe overlayers from a bcc structure in the bulk to a local hexagonal close packed (hcp) atom arrangement. In addition, the strong 3d–5d hybridization between Fe and Ir is expected to change the exchange coupling in the Fe overlayer which could lead to frustration and complex magnetic order.

The paper is organized as follows: in section 2, the experimental and theoretical techniques are introduced. The focus is on the constant-current mode of spin-resolved STM measurements used for revealing atomic scale magnetic unit cells. We consider the behavior of a FM tip in an external magnetic field and the consequences for the observed SP-STM images. Then a phenomenological view of a possible origin of collinear and non-collinear magnetic structures is given in terms of the classical Heisenberg model. To properly take into account the electronic structure of the investigated systems we use calculations based on density functional theory to treat complex non-collinear magnetic structures. Section 3 is dedicated to the experimental and theoretical results obtained for the system of Fe on Ir(111). Measurements of the electronic structure of a single Fe monolayer and a double-layer are shown. One focus of this paper is the observation of faulted and unfaulted growth of the hexagonal monolayer and the measurements of the electronic structure are compared to calculations of the vacuum density of states. The magnetic structure for both stackings is investigated experimentally and theoretically and interpreted in terms of exchange interactions. In section 4, the results are summarized and a conclusion is given.

2. Methods used to investigate the system

2.1. Experimental method and instrumentation

SP-STM has proven to be a powerful tool to study magnetism of surfaces down to the atomic scale [8, 11, 14, 18]. When using a spin-polarized probe tip the tunnel current can be described as

$$I_{\mathrm{SP}} = I_0\,[1 + P_{\mathrm{T}} \cdot P_{\mathrm{S}} \cdot \mathbf{m}_{\mathrm{T}} \cdot \mathbf{m}_{\mathrm{S}}], \tag{1}$$

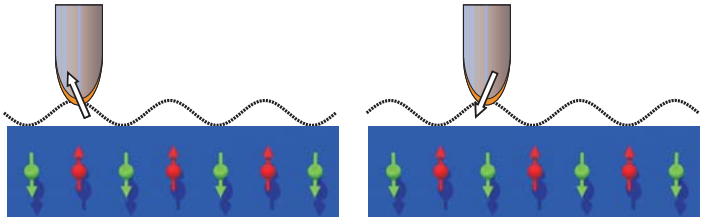

Figure 1. Constant-current mode of operation for spin-resolved STM measurements of collinear antiferromagnets. Left and right panel with different magnetization direction of the tip show the same signal with a phase shift of half a magnetic unit cell.

where I_0 is the spin-averaged tunnel current and $P_{\mathrm{T,S}}$ and $\mathbf{m}_{\mathrm{T,S}}$ are the spin polarization and the unit vectors of the magnetization of tip (T) and sample (S), respectively [18, 19]. For FM samples with different domains in the image area the spectroscopy mode can be used to extract information about the magnetization directions of the domains: variations in the differential tunneling conductance $\mathrm{d}I/\mathrm{d}U$ for electronically equivalent sample areas are then due to different relative magnetization directions of tip and sample. The spin-polarization P is energy dependent and good conditions for magnetic imaging can be identified by performing full $\mathrm{d}I/\mathrm{d}U$ spectroscopy and choosing a bias voltage U_{b} where the spin polarization of the tunnel current is large. It has been theoretically proposed [18] and experimentally demonstrated, that small magnetic unit cells can also be imaged in the constant-current mode and that the spin-polarized part may dominate for homoatomic metallic monolayers [8, 11, 14]. The path of the tip in the constant-current mode is sketched in figure 1 for an AFM arrangement of magnetic moments and a tip with magnetization pointing essentially 'up' (left) and 'down' (right). One can see that in both cases the signal is qualitatively the same but exhibits a phase shift of half a magnetic period.

The experiments were performed in a low temperature scanning tunneling microscope (STM) with tip and sample held at $T = 13\,\mathrm{K}$ [20]. A magnetic field of up to $B = \pm 2.5\,\mathrm{T}$ can be applied perpendicular to the sample surface, i.e. along the tip axis. The STM chamber is connected to an ultra-high vacuum system with standard surface preparation and analysis devices. All tips and samples are prepared *in situ*. The Ir(111) surface was cleaned by cycles of sputtering and annealing. Fe was evaporated from a rod heated by electron bombardment and deposited on to the Ir(111) surface with a rate of approx. 0.5 atomic layers (AL) per minute at slightly elevated substrate temperature. We used chemically etched tungsten tips which were flashed to high temperature *in situ*. For the spin-resolved measurements magnetic material was deposited on to the tip apex. The magnetization direction of the thin magnetic film on the tip is crucial for the investigation of the sample magnetization (see equation (1) and figure 1). While usually Fe-coated W tips are magnetized perpendicular to the tip axis, i.e. they are sensitive to the in-plane magnetization of the sample, Gd- and low coverage Cr-coated tips are magnetized along the tip axis [13]. To prove the magnetic origin of a measured feature it is possible to use an external magnetic field to induce changes in the system, for example to move domain walls in FM films [21, 22]. However, one has to keep in mind that when using FM tips the external magnetic field might change the magnetization direction of the tip as well [8, 23]. This, at first sight a drawback, can be also be taken advantage of when the magnetic structure of the sample remains unchanged

in the applied external field, as may be the case for antiferromagnets. In our experimental set-up, the available out-of-plane external magnetic field of $B = \pm 2.5\,\mathrm{T}$ is expected to leave common metallic antiferromagnets unaffected, while it is able to change the sensitivity of an Fe-coated W tip from in-plane to out-of-plane. As shown in figure 1 and previous work [8, 14] this allows the demonstration of a phase shift of half a magnetic period for collinear out-of-plane magnetic surfaces when reversing the external magnetic field using an Fe-coated W tip.

2.2. Theoretical model and computational details

Even though it is not *a priori* clear that the Heisenberg model, which is based on the interaction between localized spins on a lattice, gives an adequate description for itinerant magnets such as the 3d-transition metals, it is often used as a starting point to describe the system in terms of a few, dominant exchange interactions. In the classical Heisenberg model, the energy is given by

$$E_{\mathrm{H}} = -\sum_{i,j} J_{ij}\,\mathbf{S}_i \cdot \mathbf{S}_j. \tag{2}$$

J_{ij} denotes the magnetic exchange coupling between local spin moments $\mathbf{S}_i$ and $\mathbf{S}_j$ on arbitrary lattice sites i and j, respectively. For many systems $J_1 = J_{i,i+1}$, i.e. the nearest neighbor interaction, dominates and for positive J_1 this leads to a FM ground state as sketched in figure 2(a) for 1D, while a negative J_1 gives rise to antiparallel alignment of adjacent spins, figure 2(b). More complex magnetic states are expected when there are competing exchange interactions, for instance a FM nearest neighbor coupling and an AFM next-nearest neighbor coupling. This leads to a frustration of the system, since a perfect configuration maximizing all exchange contributions is impossible. Depending on the number and size of the competing interactions, many different configurations are possible, from a collinear magnetic ground state as sketched in figure 2(c) to a continuous rotation of spins leading to non-collinear SSs, figure 2(d). In addition to competing exchange interactions also a geometrical frustration can induce complex magnetic order in 2D: while an AFM coupling of neighboring spins on a square lattice leads to a checkerboard arrangement of magnetic moments, figure 2(e), a nearest neighbor AFM coupling on a triangular lattice leads to frustration. Depending on the interactions beyond the nearest neighbor, this can lead to different magnetic ground states such as the collinear RW-AFM state, figure 2(f) or the co-planar Néel state, figure 2(g), with an angle of 120° between adjacent moments.

All of these states can be described as flat SSs, which are the general solutions of the classical Heisenberg model, equation (2), and are given by

$$\mathbf{S}_i = S(\cos(\mathbf{q}\mathbf{R}_i), \sin(\mathbf{q}\mathbf{R}_i), 0), \tag{3}$$

where S is the value of the spin moment, $\mathbf{R}_i$ is the position of lattice site i, and the propagation direction of the spiral is given by the SS vector $\mathbf{q}$, an arbitrary vector in the 2D Brillouin zone (2D-BZ). The energy dispersion of SSs, $E(\mathbf{q})$, is related to the Fourier transformation of the exchange constants

$$E(\mathbf{q}) = -NS^2 \sum_{i \neq 0} J_{0,i} \exp(-\mathrm{i}\mathbf{q}\mathbf{R}_i), \tag{4}$$

where N is the number of lattice sites and the sum is over all neighbors of a single site chosen arbitrarily as the origin. The exchange constants can be obtained by fitting the calculated

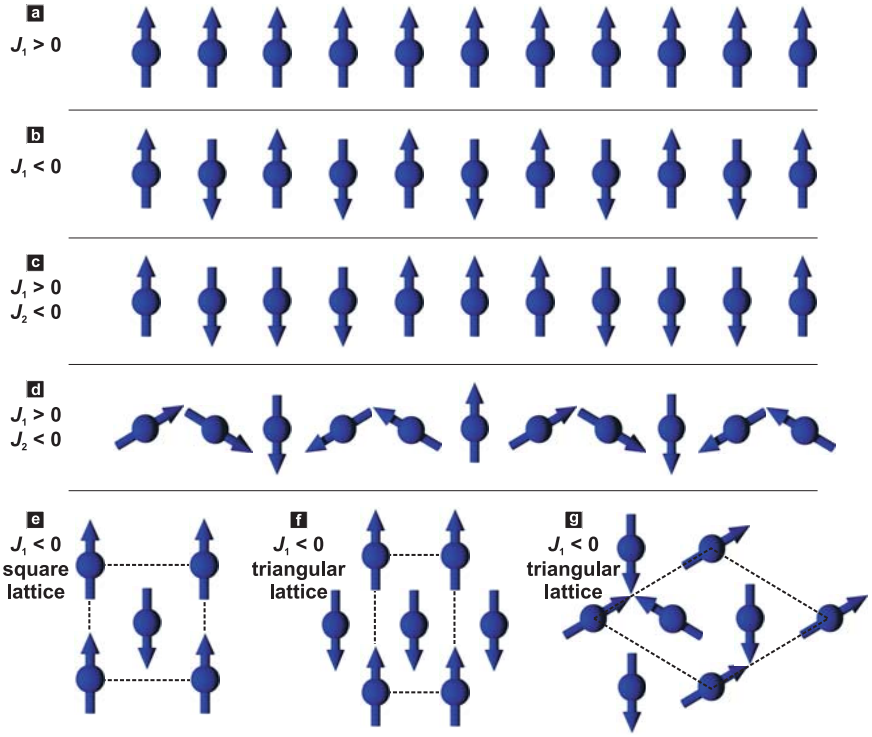

Figure 2. Competing magnetic exchange interactions and geometrical frustration. Dominating nearest neighbor exchange leads to FM (a) or AFM (b) structures but competing nearest and next-nearest neighbor exchange may lead to a variety of collinear (c) or non-collinear (d) magnetic states. While AFM nearest neighbor coupling can be realized on a square lattice (e) a hexagonal atom arrangement leads to frustration which can result, e.g. in a row-wise AFM (RW-AFM) state (f) or a non-collinear Néel state (g).

dispersions. For high symmetry points in the 2D-BZ of the hexagonal lattice, shown in figure 3, we recover well-known magnetic configurations: $\mathbf{q} = 0$, i.e. the $\overline{\Gamma}$-point, corresponds to the FM state, the $\overline{\mathrm{K}}$-point denotes the Néel state, and the $\overline{\mathrm{M}}$-point characterizes the RW-AFM state. In the 2D-BZ of the hexagonal lattice there are three equivalent $\overline{\mathrm{M}}$-points corresponding to RW-AFM states running along the three equivalent directions of the lattice. Within the Heisenberg model superpositions of such SSs corresponding to symmetry equivalent **q**-vectors, so-called multi-Q states, are energetically degenerate with the single SS. However, in itinerant magnets there can be spin interactions of higher order such as the biquadratic or the four-spin interaction which are beyond the Heisenberg model. These interactions can lift the degeneracy and favor specific multi-Q states, e.g. for 1 monolayer (ML) Mn on Cu(111) a 3Q-state, i.e. a superposition of three equivalent SSs, was predicted to be the ground state [24].

In order to understand the magnetic interactions of the system Fe on Ir(111), we have performed first-principles electronic structure calculations based on the density-functional theory. We have applied the full-potential linearized augmented plane wave (FLAPW) method as it is implemented in the FLEUR code[4]. The exchange-correlation functional has been treated

[4] http://www.flapw.de.

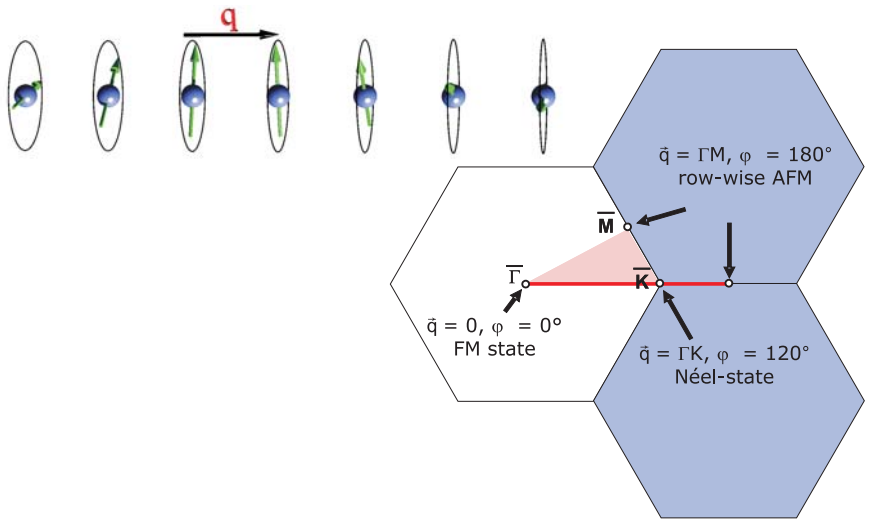

Figure 3. Sketch of a flat SS and the surface BZ for a 2D hexagonal lattice.

within the generalized-gradient approximation [25]. Within the FLEUR code, we can calculate flat SSs using the generalized Bloch theorem [26], and thus we can consider all solutions of the classical Heisenberg model in the search for the magnetic ground state. (Note that higher-order spin interactions beyond the Heisenberg model are implicitly contained in the exchange-correlation functional.) For these calculations, the surface was modeled by an asymmetric film consisting of one Fe layer in fcc or hexagonal closed packed (hcp) stacking on six layers of Ir(111). The lattice constant obtained for fcc Ir is 3.89 Å which is only 1% larger than the experimental value. The equilibrium Fe–Ir interlayer distance for the FM state is $d = 2.10$ Å for fcc-stacking and $d = 2.09$ Å for hcp-stacking. The SS calculations have been performed with 120 basis functions per atom and 1024 $\mathbf{k}_{\parallel}$ points in the full 2D-BZ. For calculations of the magnetic state containing 15 atoms in the 2D unit cell and in fcc-stacking we have used the same structural parameters as above. In the case of hcp stacking, however, we considered only four layers of the Ir(111) substrate due to the enormous computational costs. These calculations were performed using 100 basis functions per atom and six $\mathbf{k}_{\parallel}$ points in the irreducible wedge of the 2D-BZ.

3. Results

This section will first address the growth and electronic structure of Fe on Ir(111) in the low coverage regime. The magnetic properties of the fcc Fe monolayer are investigated experimentally and a model for the magnetic structure is proposed and tested based on our first-principles calculations. SS calculations are performed to scan a large portion of the magnetic phase space and to analyze the exchange interactions. Finally, the experimental observations and theoretical calculations for the two possible stackings of the Fe monolayer on Ir(111) are compared.

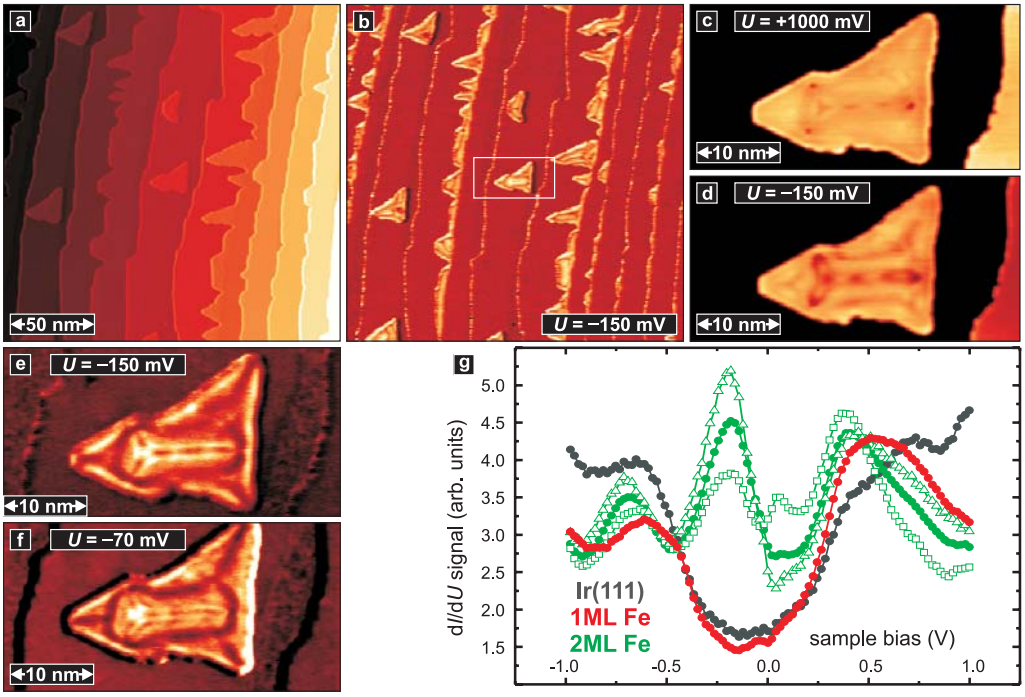

Figure 4. Topography (a) and dI/dU map (b) of 1.2 AL Fe on Ir(111) measured with a W-tip; (c), (d) topography and (e), (f) dI/dU map of the island marked in (b) at indicated sample bias; (g) dI/dU spectroscopy of the substrate, the monolayer area and the 2 ML high island shown in (c)–(f): the filled symbols represent a spectrum averaged over the whole 2 ML high island, the empty symbols show the extreme variations in the dI/dU signal with lateral position.

3.1. Growth and electronic structure in the low coverage regime

Figure 4 shows the topography (a) and a simultaneously acquired dI/dU map of 1.2 AL of Fe on the Ir(111) substrate. At this sample area, the Ir(111) surface has a terrace width of around 20 nm. It is nearly fully covered by one monolayer Fe. Only one type of stacking is observed and we believe that this is fcc while the hcp stacking is not present on this sample [14]. Islands of the second monolayer show a triangular shape, most of them are connected to step edges of the underlying Ir substrate. While the electronic structure of the Fe monolayer is spatially homogeneous as visible in the dI/dU map (figure 4(b)) the double-layer islands show variations of the differential tunneling conductance. A closer view to the isolated double-layer island marked by the white rectangle in figure 4(b) reveals that already in the topography (figure 4(c)) measured at $U = +1$ V a variation in the height is visible. We interpret this as a relaxation of the Fe double-layer due to the tensile strain of 9% (referred to nearest neighbor distance in bcc Fe and fcc Ir). While this is tolerated for the first monolayer which still grows pseudomorphic, the strain is released in the second monolayer via incorporation and rearrangement of atoms. A comparison of the topography images in figures 4(c) and (d) show that—in addition to a variation in height due to the atomic structure—the electronic structure is not homogeneous leading to the observed strong voltage-dependent appearance of the islands. Although visible in the entire studied voltage regime, this is particularly pronounced in a sample bias regime

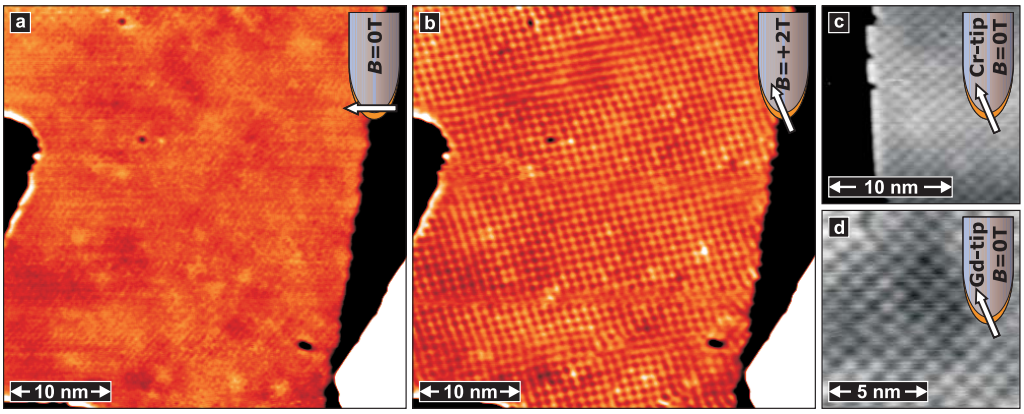

Figure 5. fcc Fe monolayer on Ir(111) measured with an Fe-coated W-tip (a) without external magnetic field and (b) at the same sample area but with external field as indicated; (c), (d) measurements without applied field with out-of-plane sensitive tips (all: $U_b = +50\,\mathrm{mV}$).

within a few hundred millivolts below the Fermi-energy (E_F), as is shown in the dI/dU maps in figures 4(e) and (f) measured at the sample bias as indicated.

The electronic structure of the Fe monolayer and the double-layer is strikingly different, as can be seen in the dI/dU spectroscopy in figure 4(g). While the Fe monolayer and the Ir(111) substrate both show one feature in the positive and one in the negative bias voltage regime, the double-layer shows an additional very pronounced peak around $U = -0.2\,\mathrm{V}$. While the dI/dU spectrum with the filled symbols shown in figure 4(g) is averaged over many points ($\sim$100 spectra) on the double-layer Fe island, the spectra with the empty symbols are taken at specific positions (averaged over ten spectra at equivalent positions). A comparison reveals that the dI/dU intensity is largely altered depending on the exact position on the island. This demonstrates the sensitivity of the dI/dU signal to the local surrounding of the atomic structure and indicates that it is responsible for the large variations in the electronic structure as seen in figures 4(c)–(f) in addition to the relaxation [27].

3.2. Magnetic imaging of the fcc Fe monolayer on Ir(111)

To investigate the magnetic properties of the Fe monolayer [14] an Fe-coated tip—sensitive to the in-plane component of the sample magnetization—was used. Without external magnetic field no distinct structure is observed as shown in the topography image in figure 5(a). When an external magnetic field of $B = +2\,\mathrm{T}$ is applied to this system a superstructure appears as shown in figure 5(b) for the same sample area. Due to this applied external field the magnetization direction of the FM Fe-coated tip is turned towards the direction of the external magnetic field, i.e. the tip axis. The observed superstructure (figure 5(b)) is of magnetic nature and can be interpreted as originating from moments being nearly parallel to the tip magnetization at high intensity and nearly antiparallel to it where a minimum is measured (see figure 1). However, the size of this superstructure does not directly correlate with the atomic distance, it does not even have the same symmetry as the hexagonal lattice: instead a nearly square magnetic unit cell of 1 nm by 1 nm is observed. Since we do not observe this superstructure without external magnetic field (figure 5(a)), i.e. with a tip sensitive to the in-plane magnetization of

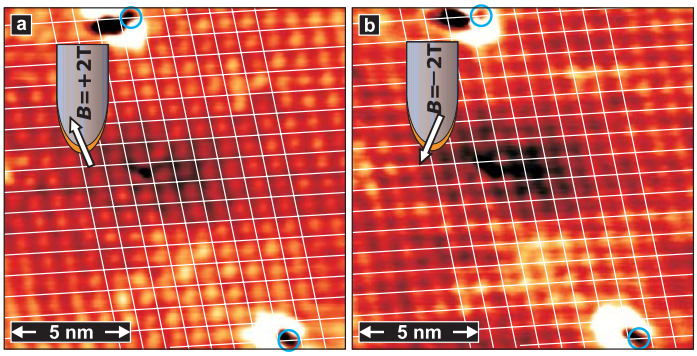

Figure 6. fcc Fe monolayer on Ir(111) measured with an Fe-coated W-tip (a) in an external magnetic field of +2 T, (b) same sample area in reversed magnetic field (both: $U_b = +50$ mV).

the sample, but only with a tip magnetization turned towards the tip axis (figure 5(b)), so that the tip becomes sensitive to the out-of-plane component of sample magnetization, we conclude that the Fe monolayer on Ir(111) exhibits a collinear out-of-plane magnetic structure. We can exclude the formation of the magnetic structure due to the external magnetic field by performing measurements with magnetically coated tips that are sensitive to the out-of-plane direction of sample magnetization without external magnetic field, as shown in figures 5(c) and (d): the same magnetic structure is observed with out-of-plane sensitive, Cr- or Gd-coated tips in zero magnetic field.

Figure 6 shows an experimental set-up to obtain additional proof that the observed superstructure is not due to a reconstruction, the adsorption of atoms or induced by the external magnetic field. The topography images show an identical sample area imaged with an Fe-coated tip in positive (figure 6(a)) and negative (figure 6(b)) magnetic field. Qualitatively the images look the same and in both cases the magnetic superstructure as in figures 5(b)–(d) is observed. Since bright and dark spots seem to be of the same size, we expect that the structure has no total magnetic moment but is compensated within one unit cell. For a collinear out-of-plane magnetic structure as proposed from the observations in figure 5 a phase shift of half a magnetic period is expected, when the out-of-plane component of the tip magnetization is reversed (see figure 1). This can be checked with the grid lines in both images: they are connected to the position of the adsorbates marked by the blue circles. In figure 6(a), the maxima of the magnetic structure are in between the grid lines, while with reversed out-of-plane component of the tip magnetization (figure 6(b)) the maxima are now on the grid lines, proving that there is indeed a magnetic phase shift of half a magnetic unit cell.

3.3. Mosaic structure: magnetic structure model on the basis of experimental results

The combination of these experimental findings—a collinear out-of-plane magnetic structure with compensated moments—leads to a model of the magnetic unit cell as shown in figure 7. Although it represents only a first collinear approach to the real, probably more complex spin structure of Fe on Ir(111), this model is in excellent agreement with the observed unit cell, which is almost a square with one diagonal along the close packed row and a lattice parameter of 1.0 nm. The proposed unit cell has a lattice parameter of $\sqrt{13}\,a = 0.979$ nm (with $a = 0.2715$ Å the surface nearest neighbor distance) and an angle of $\pm 46.1^\circ$ with respect to the close packed

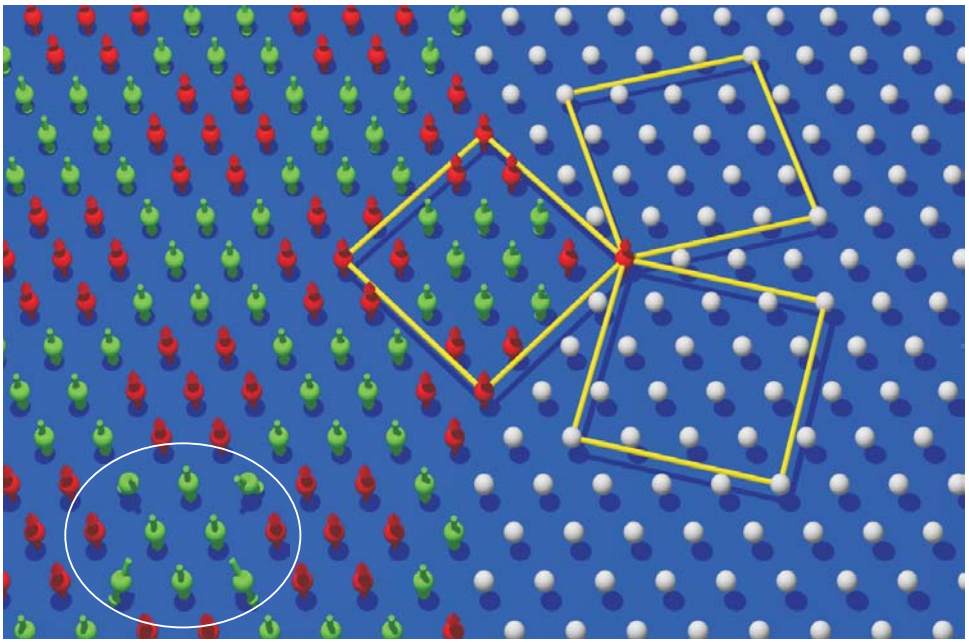

Figure 7. Mosaic structure: magnetic structure of the fcc Fe monolayer on Ir(111) proposed on the basis of the experimental results. The unit cell consists of 15 atoms, with seven spins in one direction (red) and eight spins in the opposite direction (green). Three rotational domains are possible. To construct a truly balanced structure a canting of some moments is suggested as sketched exemplarily for one cell indicated by the white ellipse.

rows. The unit cell consists of 15 atoms (see yellow lines in figure 7) with seven moments pointing in one direction (red) and eight moments pointing in the opposite direction (green). Due to symmetry reasons three rotational domains are possible, all of which are observed experimentally [14]. While the condition of collinear out-of-plane moments is fulfilled in this model, the moments of this structure are not fully balanced when a constant magnetic moment for all Fe atoms is assumed. Two possible scenarios come to mind to bring this model structure into accordance with a fully compensated structure: firstly, not all Fe atoms have the same moments, and secondly, some moments are canted resulting in a reduced out-of-plane moment for the group of eight. In the first case a variation of the moments of less than 7% would be sufficient to achieve full compensation: 16/15 of a given moment for the group of seven and 14/15 of the magnetic moments for the group of eight compared to a constant moment. The second scenario would imply a canting of some moments as sketched exemplarily inside the white ellipse of figure 7. To achieve a compensated structure for the suggested configuration a spin canting of 40° would be needed for each of those four atoms. In the magnetically inhomogeneous surrounding of the individual atoms such a variation of the size and/or the direction of the magnetic moment may be possible. In the following we will call the collinear model structure as sketched in figure 7 the AFM 7 : 8 structure.

In order to check whether the electronic structure of the proposed AFM 7 : 8 structure is consistent with the experimental observations, we have performed first-principles calculations of an fcc monolayer Fe on Ir(111). Indeed, this unusual magnetic state turns out to be energetically favorable by a significant energy difference of 9.8 meV per Fe atom as compared

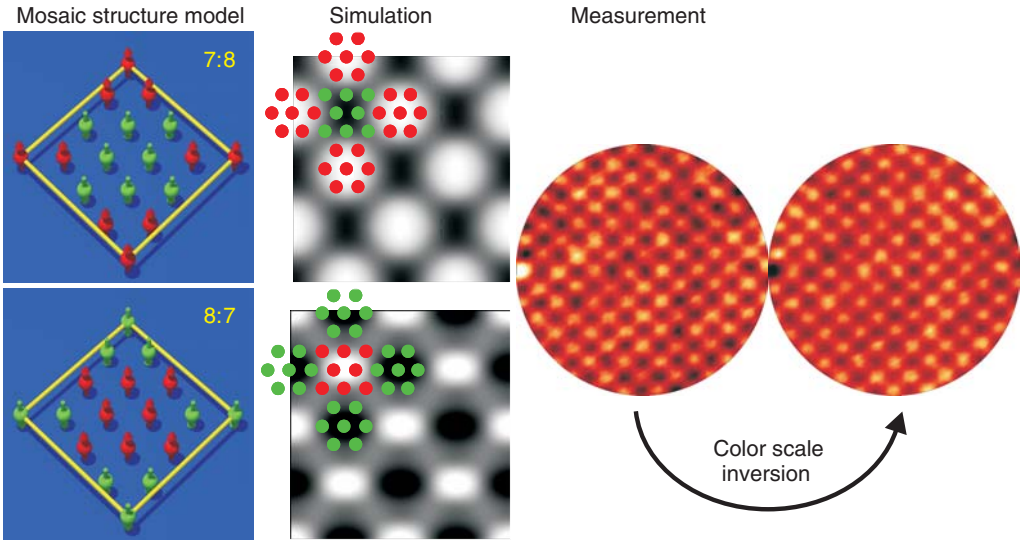

Figure 8. Mosaic structure model and calculated SP-STM images for a 7 : 8 configuration of spins (upper panel) and a 8 : 7 configuration (lower panel), and measured SP-STM data. Note that the SP-STM images stem from only one data-set which is subjected to a color scale inversion from upper to lower panel.

to the FM state[5]. The magnitude of the magnetic moments in the Fe monolayer is nearly constant with values of $m_{\mathrm{Fe}} = 2.92 \pm 0.06\,\mu_{\mathrm{B}}$ and the total moment of the unit cell is $2.6\,\mu_{\mathrm{B}}$. A slight artificial reduction of the interlayer distance between the Fe monolayer and the Ir(111)-surface in our calculation leads to a large energy gain of the AFM 7 : 8 state with respect to the FM configuration. This indicates the crucial role played by the hybridization for the magnetic interactions in this system. Their nature is studied in more detail in the following sections.

To further investigate a possible uncompensated spin moment in the mosaic structure, spin-resolved STM images of collinear magnetic structures have been calculated based on the spin-polarized version of the Tersoff–Hamann model [18]. Figure 8 shows the model of the mosaic structure (left) and the calculation (center) with (7 : 8) moments in the upper panel and (8 : 7) moments, i.e. the other possible domain, in the lower panel. The calculations are both in reasonable agreement with the experimental data, but they show that experimentally a distinction between these two structures could be difficult. On the right side of figure 8 a topography image of the Fe monolayer on Ir(111) is shown. A color scale inversion of this image is displayed next to it and the comparison clearly demonstrates, that the images look identical except for a phase shift due to the inversion, which means that the observed structure is symmetric with respect to the surface plane. This suggests compensated moments for the observed magnetic mosaic structure. The uncompensated total moment calculated for the AFM 7 : 8 state hints at a non-collinear structure with a slight canting of a few magnetic

[5] In [14] we could consider only four layers of Ir(111) and the energy gain of the MS was only 3 meV per atom while it increased here to 9.8 meV per atom due to the use of a six layer Ir(111) substrate. This indicates some influence of quantum well states confined in the Ir substrate. However, our key conclusions are independent of these effects, in particular the 7 : 8 AFM state remains the global ground state and the SS dispersions are almost unaffected close to the $\overline{\Gamma}$ point.

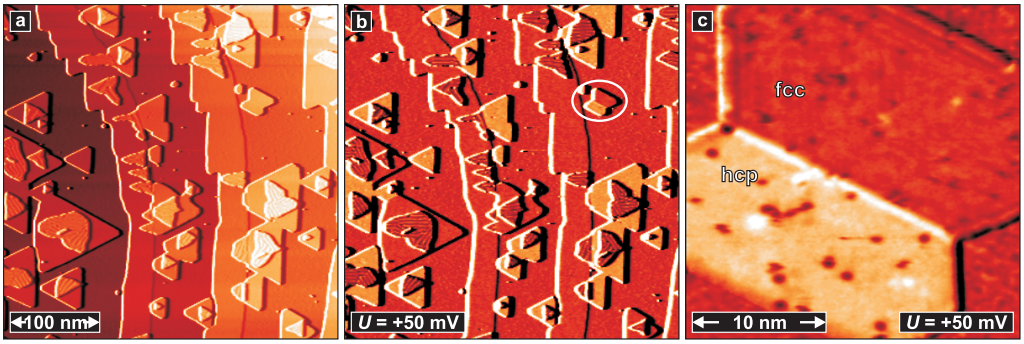

Figure 9. Topography (a) and dI/dU map (b) of 0.7 AL Fe on Ir(111); (c) dI/dU map of the island marked in (b).

moments. Simulations of SP-STM images using a simple model [17] are in agreement with such a structure.

3.4. Electronic structure of the fcc and hcp Fe monolayer: experiment and calculation

Samples with a coverage below 1 AL—such as the one displayed in figure 9—show Fe monolayer patches which can grow in two different in-plane commensurate stackings, fcc and hcp. Additionally, we can see that the step edges are decorated with about 30 nm wide rims of Fe. The fcc and hcp islands can be distinguished in the topography image (figure 9(a)) and the corresponding dI/dU map (figure 9(b)). The triangular shape of isolated islands is characteristic, with the two different types always pointing in opposite directions. In the dI/dU map at +50 mV in figure 9(b) and the closer view of the encircled island in figure 9(c) one can see that the stackings can be distinguished by their different electronic structure, which causes one to appear brighter than the other. The Fe grown at the step edges of the Ir(111) substrate is always the darker type. In contrast, the islands on the terraces are more often of the brighter type. This indicates that the Fe monolayer areas connected to the step edges grow kinetically induced and continue the atom arrangement of the Ir atoms, and they are the ones which we identified as fcc. The monolayer type grown on the terraces is then the thermodynamically stable configuration which we believe to be hcp in this case. Our interpretation is supported by the first-principles calculations which favor the hcp-stacking by 7.6 meV per Fe atom in the FM state.

Figure 10(a) shows the experimental spectra of both types of Fe monolayers which possess two distinct features in the occupied and unoccupied density of states at about ±0.5 V. There is a clear shift of the unoccupied peak between the two stackings. Within the Tersoff–Hamann model [28] of STM we can directly compare these experimental spectra with the *ab initio* calculated local density of states (LDOS) in the vacuum, figure 10(b). In the calculation, we have considered different magnetic solutions for both types of stackings. For the FM state, we observe a very sharp peak at an energy of about +0.25 eV above the Fermi level, E_F, with a very small shift between the fcc and hcp stacking. For the AFM 7 : 8 structure, which serves as a model for the mosaic state (MS), the LDOS looks strikingly different. We find a narrow peak at an energy of about $E_F - 0.35$ eV for both stackings, while a broad feature is obtained in the unoccupied states. It is shifted from +0.65 to +0.55 eV when we compare the fcc to the hcp stacking. This double peak structure with a broad feature in the unoccupied states and

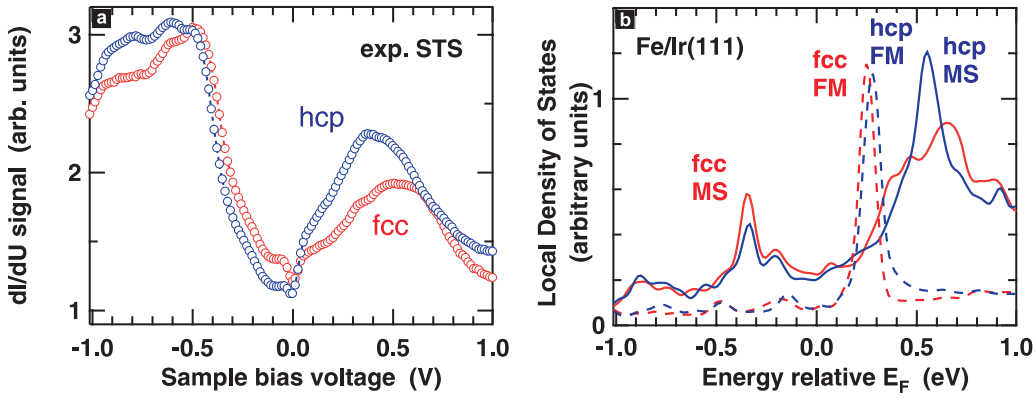

Figure 10. Comparison of the experimental spectra with the calculated LDOS in the vacuum for different magnetic configurations. (a) Experimental spectra for the two types of stackings. (b) Calculated LDOS in the vacuum at a distance of 7.2 Å for fcc and hcp stacking in the FM state and in the AFM 7 : 8 model MS. (LDOS of the MS state is taken from calculations with four layers of Ir(111).)

an energy difference of 1 eV between the peaks is in good agreement with the experimental observation. The relative peak intensities are different in the experiment, however, this depends on the tip electronic structure. For example, in the spectrum shown in figure 4(g) the ratio of the peak heights is reversed. In addition, the shift of the unoccupied peak is clearly visible in both experiment and calculation, cf figure 10. We conclude that the observed spectra are consistent with the proposed MS, for both types of stackings. (We have also found the MS to be more favorable than the FM state for hcp stacking of the Fe monolayer by about 16 meV per Fe atom using four layers of Ir(111) substrate.)

3.5. SS calculations for the Fe monolayer on Ir(111)

So far, we have considered only two collinear magnetic structures in our calculations. However, in principle an infinite number of magnetic configurations is possible. In order to take into account an important part of the phase space we have performed SS calculations which cover all solutions within the classical Heisenberg model. In addition, the mapping to a classical Heisenberg Hamiltonian allows us to interpret our results within the picture of exchange couplings between pairs of local moments.

Figure 11(a) displays the dispersion relation of flat SSs (equation (3)) as a function of the spiral vector **q** along the high symmetry lines of the 2D-BZ (figure 3) for an hexagonal Fe monolayer in different environments. For an unsupported monolayer (UML) the lowest energy is obtained at the $\overline{\Gamma}$-point, corresponding to the FM state, and the energy rises quickly with increasing length of **q**. This behavior characterizes strong FM coupling of nearest neighbor magnetic moments. When we compare an UML of iron with an Fe monolayer on the Ag(111) surface, we find that the SS dispersion and thus the magnetic coupling is unaltered in the vicinity of $\overline{\Gamma}$, although the magnetic moment is considerably reduced from 3.04 μ_B for the UML to 2.93 μ_B on Ag(111) due to hybridization.

The situation changes dramatically on the Ir(111) surface. For both types of stackings, the energy difference between spirals at the high symmetry points of the 2D-BZ is strongly reduced

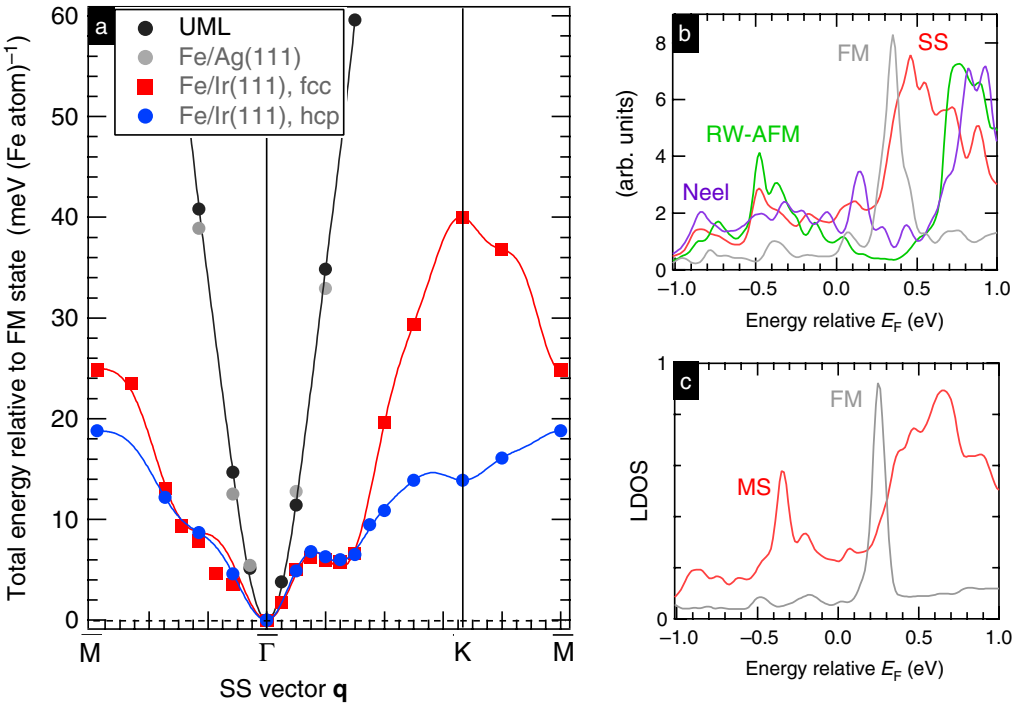

Figure 11. Calculated dispersion of flat SSs for an hexagonal Fe monolayer in different environments and LDOS in the vacuum. (a) Dispersion relation for an unsupported hexagonal Fe monolayer (unsupported monolayer (UML)) with the Ir lattice constant, an Fe monolayer on the Ag(111) surface and in fcc and hcp stacking on the Ir(111) surface. Calculations have been performed for an Fe–Ir interlayer distance corresponding to the relaxed value in the FM state and six layers of the Ir(111) substrate. LDOS in the vacuum for the fcc Fe monolayer/Ir(111) at a distance of 7.2 Å from the surface for (b) SSs with wavevectors of **q** corresponding to the $\overline{\Gamma}$-point (FM, gray line), the $\overline{\mathrm{K}}$-point (Néel state, blue line), the $\overline{\mathrm{M}}$-point (RW-AFM, green line), and $\mathbf{q} = 0.25\,\overline{\Gamma\mathrm{KM}}$ (SS, red line) and (c) the FM and the (7 : 8) AFM MS (as in figure 10(b)).

indicating a lowering of the nearest neighbor exchange coupling J_1. Indeed, from a fitting of the curves with the Heisenberg model we find J_1 to be still FM, but reduced by a factor of about five for the fcc-stacking compared to the UML. For the hcp-stacking this reduction of J_1 is even stronger. Due to the small nearest-neighbor exchange interaction, several magnetic interactions can be of comparable strength and complex magnetic structures may occur [10]. Nevertheless the FM state remains the global energy minimum of all spin spirals and is the ground state within the Heisenberg model. Note, that in the first-principles calculations the total energy of the AFM 7 : 8 state was found to be even lower than the energy of the FM state and must be stabilized by interactions beyond the Heisenberg model.

Close to $\overline{\Gamma}$ the dispersion curves look similar for both stackings, in particular, a local energy minimum can be observed for $\mathbf{q} \approx 0.25\,\overline{\Gamma\mathrm{KM}}$ located only 6 meV per Fe atom above the FM state. In the direction $\overline{\Gamma\mathrm{M}}$, there is also a shoulder in the curves at a similar absolute value of **q**. For this value of $|\mathbf{q}|$, the energy remains nearly constant on a ring in the 2D-BZ connecting

the two points on the high symmetry lines [14]. Interestingly, the value of $|\mathbf{q}|$ on this ring-like local energy minimum corresponds to real space SSs with a period of 1.1 nm, close to the lattice constant of the experimentally observed magnetic structure.

As discussed in section 2.2, linear combinations of SSs, so-called multi-Q states, can gain energy due to higher order spin interactions. The energy due to such terms can be on the order of 15 meV atom^{-1} as has been calculated for 1 ML Mn on Cu(111) [24]. It is possible that SSs on the ring-like energy plateau at $|\mathbf{q}| \approx 0.25\,\overline{\Gamma\mathrm{KM}}$, can form multi-Q states with the same 2D unit cell as the MS and compensated magnetic moments. This could also remove some frustration from the uncompensated collinear AFM 7 : 8 state, which is probably only a collinear approximation of a more complex, non-collinear magnetic arrangement which forms the mosaic structure.

The connection between SSs at the local energy minimum and the MS can also be observed in the electronic structure. While the vacuum LDOS for SSs, figure 11(b), corresponding to the Néel and the RW-AFM state display distinctive unoccupied peaks at +0.85 eV and +0.75 eV, respectively, the SS with $|\mathbf{q}| = 0.25\,\overline{\Gamma\mathrm{KM}}$ possesses a double peak structure in close resemblance to the AFM 7 : 8 state, cf figure 11(c). Even the absolute peak positions are in good agreement with the experiment, but is has to be noted that the exact energetic positions depend also on the thickness of the Ir(111) substrate used in the calculations.

To conclude this section, we emphasize that the hybridization between the 3d-states of Fe and the 5d-states of Ir is responsible for the strong suppression of the nearest-neighbor exchange interaction in the Fe monolayer. This dramatic modification enables exchange interactions beyond nearest-neighbors or even spin interactions of higher order to play a crucial role in determining the magnetic ground state of the system. Predictions are therefore difficult since very accurate values for all competing terms are required which are only on the order of a few millielectronvolts. The exchange interactions for fcc- and hcp-stacking of the Fe monolayer are quite similar and in both cases we find the unusual MS to be significantly lower in total energy than all solutions of the Heisenberg model. However, for hcp-stacking the nearest-neighbor FM exchange is even smaller than for fcc which may lead to many metastable states very close in total energy.

3.6. Magnetic imaging of the hcp Fe monolayer on Ir(111)

Figure 12 shows a spin-resolved measurement of a sample with fcc and hcp areas. An overview of the topography is shown in figure 12(a) with the corresponding $\mathrm{d}I/\mathrm{d}U$ map in figure 12(d). The closer views in figures 12(b) and (c) are higher resolved images taken at the areas marked in figure 12(a) by the black boxes with the color scale adjusted to show the details of the monolayer areas. While in the fcc monolayer the mosaic structure is clearly resolved, a magnetic superstructure is not as obvious for the hcp areas. Only in the fully differentiated images of the same areas in figures 12(e) and (f) one can see a similar magnetic structure, which is very faint and even disappears when going away from the borders of the patches. It seems as if the magnetic structure was induced by the fcc monolayer and double-layer areas connected with the hcp area, but not as if it were a stable magnetic structure at the measuring temperature of 13 K. The magnetic signal appears to vanish towards the center of the hcp monolayer. This indicates that the mosaic structure or a related magnetic structure is one out of several possible magnetic states in the hcp monolayer, but it needs to be stabilized by an adjacent fcc monolayer or by double-layer patches. This might reflect the very small energy differences calculated in the

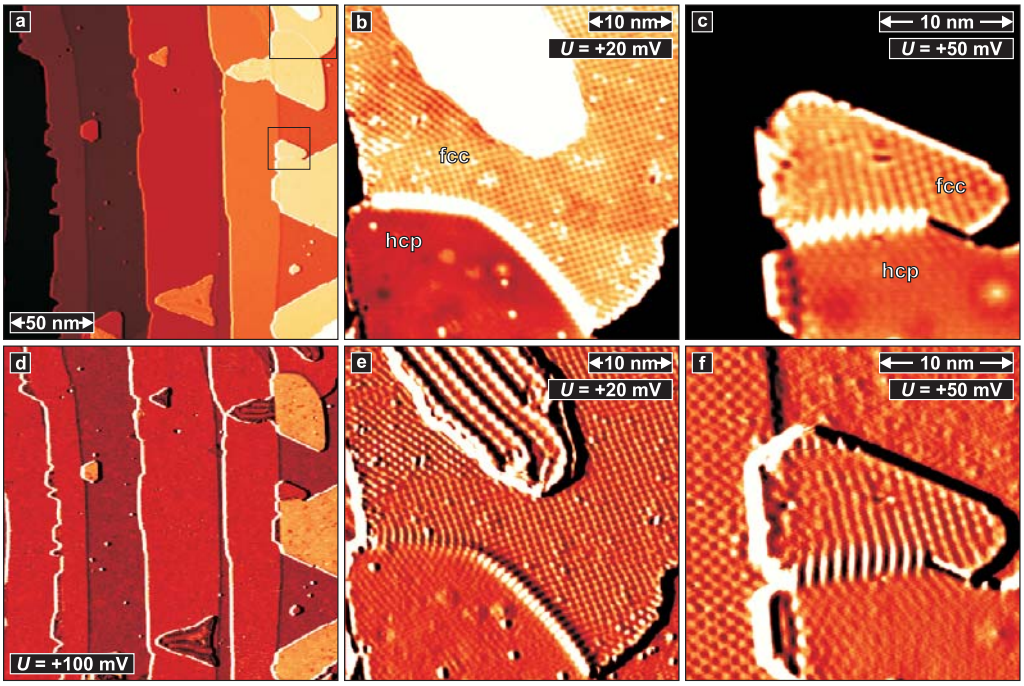

Figure 12. fcc and hcp Fe monolayer on Ir(111): (a) topography and (d) corresponding dI/dU map; (b), (c) spin-sensitive images in indicated areas of (a) and (e), (f) same areas but fully differentiated for better visibility of height variations in fcc and hcp monolayer in one image.

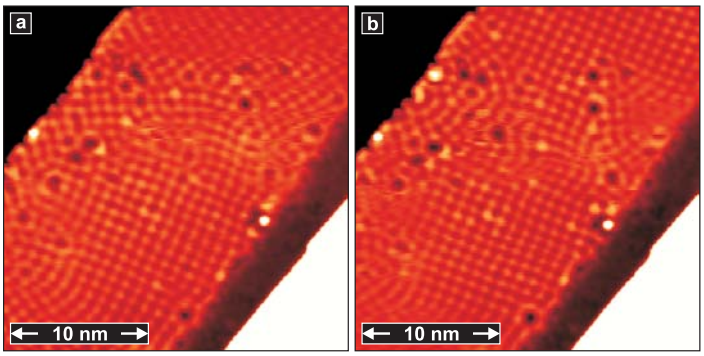

Figure 13. fcc Fe monolayer on Ir(111) measured with an Fe-coated W-tip at $B = +2$ T. (a) and (b) are measured at the same sample area with a time interval of 4 min (both: $U_b = +50$ mV).

energy dispersion of the spin spirals and the correspondingly small nearest-neighbor exchange interaction (figure 11(a)).

Considering the previous result raises also the question of the stability of a magnetic structure and its imaging by SP-STM. Figure 13 shows two subsequently acquired spin-resolved topography images of the fcc monolayer. All three possible rotational domains are present in figure 13(a), merging into one another on a rather small scale. As can be seen in the top part of the image the mosaic structure seems to be blurred and the spin-resolved contrast is not

as clear as in the previously shown images, even though one can still see which domain is present. In the following image figure 13(b), acquired only a few minutes later, the domain structure at the bottom of the image has remained unchanged, while the middle part and—more obvious—the top domain has spontaneously rotated. This was more often observed for such small domains rather than for extended domains in the fcc monolayer. This behavior suggests an alternative explanation why no magnetic superstructure was observed in the hcp monolayer: if spontaneous changes—a lateral phase shift or a rotation of the domains—occur with a high frequency compared to the measurement time, it could be possible that the same mosaic structure, that was observed on fcc stacking, is also the magnetic ground state for the hcp layers, but just cannot be imaged due to spatial high-frequency fluctuations of the magnetic pattern.

4. Summary and conclusion

We have investigated the growth of Fe on Ir(111) and its electronic and magnetic properties in the low coverage regime: while an Fe monolayer grows in-plane commensurate in the two different stackings, fcc and hcp, a second atomic layer on top of this commensurate layer relaxes and shows a distinct electronic structure. The electronic structure of fcc and hcp stacked monolayers is very similar, characterized by two peaks, one at -0.5 V and a broader one at around $+0.5$ V and $+0.4$ V for fcc and hcp, respectively. The magnetic superstructure observed experimentally for fcc monolayer areas leads to the proposition of the mosaic structure. Our first-principles calculations show that indeed the energy of a collinear approximation to the mosaic structure is lower than that of the FM state by 9.8 and 16 meV per atom for the fcc and hcp state, respectively. The comparison with the calculated vacuum density of states further supports the model of this novel magnetic structure, since good agreement is observed between $\mathrm{d}I/\mathrm{d}U$ spectra of the fcc monolayer and the calculated vacuum density of states of this mosaic structure, while the calculated LDOS of the FM state looks significantly different. The same holds for the comparison of the spectra of the hcp monolayer with the calculated vacuum density of states.

From SS calculations we find a strongly reduced FM nearest-neighbor exchange interaction which allows terms beyond nearest neighbors as well as higher order spin interactions beyond the Heisenberg model to influence the magnetic ground-state. The absolute value of the wave vector $|\mathbf{q}|$ at the ring-like local energy minimum in the SS calculations is in good agreement with the experimentally observed periodicity for the mosaic structure. This allows to construct non-collinear states with the same unit cell as the MS and a similar electronic structure. The SS calculations further suggest that both stackings have similar magnetic properties and the calculation of the vacuum density of states indicates that the ground state of both fcc and hcp is the mosaic structure. While this was experimentally found for the fcc monolayer, for hcp it seems like the mosaic structure can be induced, but is not stable enough to be observed in larger hcp areas. Two possible explanations are discussed: a small energy barrier for a phase shift or a rotation of the mosaic structure, or small energy differences to other possible magnetic states for hcp stacking. The latter is supported by the shallow energy dispersion of the SSs, which might allow the formation of other, non-collinear magnetic states with similar energies.

Acknowledgments

Financial support from the DFG (SFB 668), the Stifterverband für die Deutsche Wissenschaft, and the Interdisciplinary Nanoscience Center of Hamburg is gratefully acknowledged.

References

[1] Kortright J, Awschalom D, Stöhr J, Bader S, Idzerda Y, Parkin S, Schuller I K and Siegmann H-C 1999 *J. Magn. Magn. Mater.* **207** 7
[2] Fassbender J 2003 *Top. Appl. Phys.* **87** 59
[3] Fruchart O and Thiaville A 2005 *C R Physique* **6** 921
[4] Harrison R 2006 Newtron diffractron of magnetic materials *Neutron Scattering in Earth Sciences* (*Reviews in Mineralogy and Geochemistry* vol 63) ed H-R Weull (Chantilly, VA: MSA) chapter 6, p 113
[5] Srajer G *et al* 2006 *J. Magn. Magn. Mater.* **307** 1
[6] Tsunoda Y 1989 *J. Phys.: Condens. Matter* **1** 10427
[7] Knöpfle K, Sandratskii L M and Kübler J 2000 *Phys. Rev.* B **62** 5564
[8] Kubetzka A, Ferriani P, Bode M, Heinze S, Bihlmayer G, von Bergmann K, Pietzsch O, Blügel S and Wiesendanger R 2005 *Phys. Rev. Lett.* **94** 087204
[9] Bode M, Vedmedenko E Y, von Bergmann K, Kubetzka A, Ferriani P, Heinze S and Wiesendanger R 2006 *Nat. Mater.* **5** 477
[10] Ferriani P, Turek I, Heinze S, Bihlmayer G and Blügel S 2007 *Phys. Rev. Lett.* at press (*Preprint* cond-mat/0701241v1)
[11] Heinze S, Bode M, Kubetzka A, Pietzsch O, Nie X, Blügel S and Wiesendanger R 2000 *Science* **288** 1805
[12] Yang H, Smith A R, Prikhodko M and Lambrecht W R L 2002 *Phys. Rev. Lett.* **89** 226101
[13] Bode M 2003 *Rep. Prog. Phys.* **66** 523
[14] von Bergmann K, Heinze S, Bode M, Vedmedenko E Y, Bihlmayer G, Blügel S and Wiesendanger R 2006 *Phys. Rev. Lett.* **96** 167203
[15] Gao C L, Schlickum U, Wulfhekel W and Kirschner J 2007 *Phys. Rev. Lett.* **98** 107203
[16] Bode M, Heide M, von Bergmann K, Ferriani P, Heinze S, Bihlmayer G, Kubetzka A, Pietzsch O, Blügel S and Wiesendanger R 2007 *Nature* **447** 190
[17] Heinze S 2006 *Appl. Phys.* A **85** 407
[18] Wortmann D, Heinze S, Kurz P, Bihlmayer G and Blügel S 2001 *Phys. Rev. Lett.* **86** 4132
[19] Slonczewski J C 1989 *Phys. Rev.* B **39** 6995
[20] Pietzsch O, Kubetzka A, Haude D, Bode M and Wiesendanger R 2000 *Rev. Sci. Instrum.* **71** 424
[21] Kubetzka A, Bode M, Pietzsch O and Wiesendanger R 2002 *Phys. Rev. Lett.* **88** 057201
[22] Bode M, Heinze S, Kubetzka A, Pietzsch O, Nie X, Bihlmayer G, Blügel S and Wiesendanger R 2002 *Phys. Rev. Lett.* **89** 237205
[23] Pietzsch O, Kubetzka A, Bode M and Wiesendanger R 2001 *Science* **292** 2053
[24] Kurz P, Bihlmayer G, Hirai K and Blügel S 2001 *Phys. Rev. Lett.* **86** 1106
[25] Perdew J P, Burke K and Ernzerhof M 1996 *Phys. Rev. Lett.* **77** 3865
[26] Kurz P, Förster F, Nordström L, Bihlmayer G and Blügel S 2004 *Phys. Rev.* B **69** 024415
[27] Meier F, von Bergmann K, Ferriani P, Wiebe J, Bode M, Hashimoto K, Heinze S and Wiesendanger R 2006 *Phys. Rev.* B **74** 195411
[28] Tersoff J and Hamann D R 1985 *Phys. Rev.* B **31** 805